# Terahertz Spectroscopy

## PRINCIPLES AND APPLICATIONS

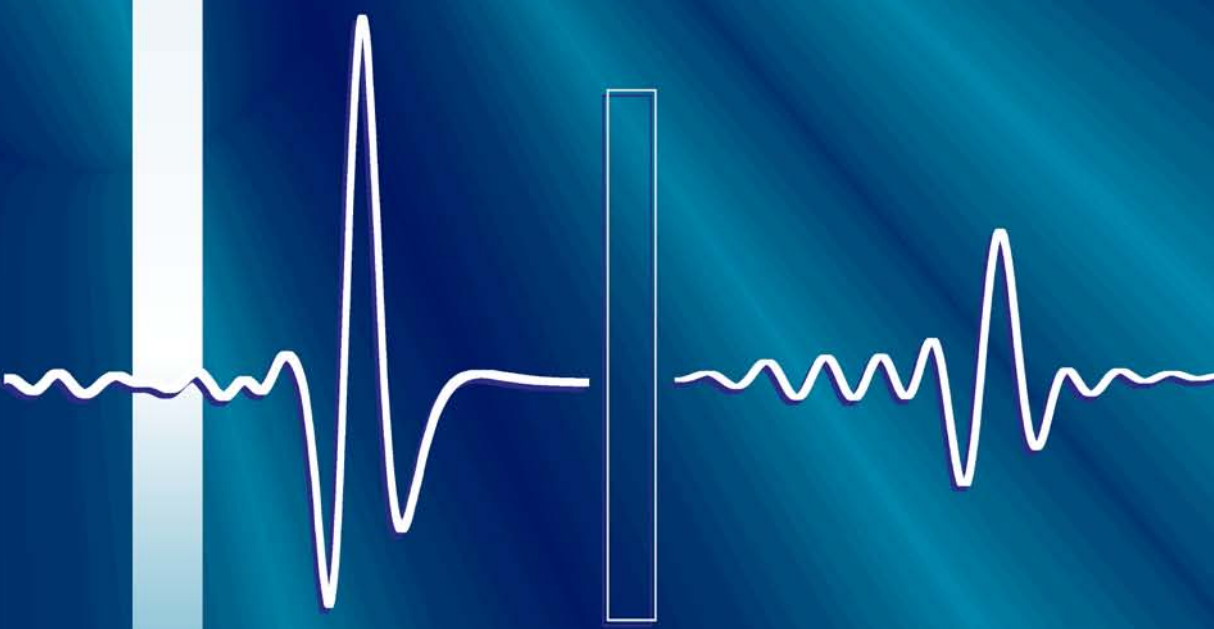

Edited by Susan L. Dexheimer

CRC Press
Taylor & Francis Group

# Terahertz Spectroscopy

## PRINCIPLES AND APPLICATIONS

# OPTICAL SCIENCE AND ENGINEERING

*Founding Editor*
**Brian J. Thompson**
*University of Rochester*
*Rochester, New York*

1. Electron and Ion Microscopy and Microanalysis: Principles and Applications, *Lawrence E. Murr*
2. Acousto-Optic Signal Processing: Theory and Implementation, *edited by Norman J. Berg and John N. Lee*
3. Electro-Optic and Acousto-Optic Scanning and Deflection, *Milton Gottlieb, Clive L. M. Ireland, and John Martin Ley*
4. Single-Mode Fiber Optics: Principles and Applications, *Luc B. Jeunhomme*
5. Pulse Code Formats for Fiber Optical Data Communication: Basic Principles and Applications, *David J. Morris*
6. Optical Materials: An Introduction to Selection and Application, *Solomon Musikant*
7. Infrared Methods for Gaseous Measurements: Theory and Practice, *edited by Joda Wormhoudt*
8. Laser Beam Scanning: Opto-Mechanical Devices, Systems, and Data Storage Optics, *edited by Gerald F. Marshall*
9. Opto-Mechanical Systems Design, *Paul R. Yoder, Jr.*
10. Optical Fiber Splices and Connectors: Theory and Methods, *Calvin M. Miller with Stephen C. Mettler and Ian A. White*
11. Laser Spectroscopy and Its Applications, *edited by Leon J. Radziemski, Richard W. Solarz, and Jeffrey A. Paisner*
12. Infrared Optoelectronics: Devices and Applications, *William Nunley and J. Scott Bechtel*
13. Integrated Optical Circuits and Components: Design and Applications, *edited by Lynn D. Hutcheson*
14. Handbook of Molecular Lasers, *edited by Peter K. Cheo*
15. Handbook of Optical Fibers and Cables, *Hiroshi Murata*
16. Acousto-Optics, *Adrian Korpel*
17. Procedures in Applied Optics, *John Strong*
18. Handbook of Solid-State Lasers, *edited by Peter K. Cheo*
19. Optical Computing: Digital and Symbolic, *edited by Raymond Arrathoon*
20. Laser Applications in Physical Chemistry, *edited by D. K. Evans*
21. Laser-Induced Plasmas and Applications, *edited by Leon J. Radziemski and David A. Cremers*

22. Infrared Technology Fundamentals, *Irving J. Spiro and Monroe Schlessinger*
23. Single-Mode Fiber Optics: Principles and Applications, Second Edition, Revised and Expanded, *Luc B. Jeunhomme*
24. Image Analysis Applications, *edited by Rangachar Kasturi and Mohan M. Trivedi*
25. Photoconductivity: Art, Science, and Technology, *N. V. Joshi*
26. Principles of Optical Circuit Engineering, *Mark A. Mentzer*
27. Lens Design, *Milton Laikin*
28. Optical Components, Systems, and Measurement Techniques, *Rajpal S. Sirohi and M. P. Kothiyal*
29. Electron and Ion Microscopy and Microanalysis: Principles and Applications, Second Edition, Revised and Expanded, *Lawrence E. Murr*
30. Handbook of Infrared Optical Materials, *edited by Paul Klocek*
31. Optical Scanning, *edited by Gerald F. Marshall*
32. Polymers for Lightwave and Integrated Optics: Technology and Applications, *edited by Lawrence A. Hornak*
33. Electro-Optical Displays, *edited by Mohammad A. Karim*
34. Mathematical Morphology in Image Processing, *edited by Edward R. Dougherty*
35. Opto-Mechanical Systems Design: Second Edition, Revised and Expanded, *Paul R. Yoder, Jr.*
36. Polarized Light: Fundamentals and Applications, *Edward Collett*
37. Rare Earth Doped Fiber Lasers and Amplifiers, *edited by Michel J. F. Digonnet*
38. Speckle Metrology, *edited by Rajpal S. Sirohi*
39. Organic Photoreceptors for Imaging Systems, *Paul M. Borsenberger and David S. Weiss*
40. Photonic Switching and Interconnects, *edited by Abdellatif Marrakchi*
41. Design and Fabrication of Acousto-Optic Devices, *edited by Akis P. Goutzoulis and Dennis R. Pape*
42. Digital Image Processing Methods, *edited by Edward R. Dougherty*
43. Visual Science and Engineering: Models and Applications, *edited by D. H. Kelly*
44. Handbook of Lens Design, *Daniel Malacara and Zacarias Malacara*
45. Photonic Devices and Systems, *edited by Robert G. Hunsberger*
46. Infrared Technology Fundamentals: Second Edition, Revised and Expanded, *edited by Monroe Schlessinger*
47. Spatial Light Modulator Technology: Materials, Devices, and Applications, *edited by Uzi Efron*
48. Lens Design: Second Edition, Revised and Expanded, *Milton Laikin*
49. Thin Films for Optical Systems, *edited by Francoise R. Flory*
50. Tunable Laser Applications, *edited by F. J. Duarte*
51. Acousto-Optic Signal Processing: Theory and Implementation, Second Edition, *edited by Norman J. Berg and John M. Pellegrino*

52. Handbook of Nonlinear Optics, *Richard L. Sutherland*
53. Handbook of Optical Fibers and Cables: Second Edition, *Hiroshi Murata*
54. Optical Storage and Retrieval: Memory, Neural Networks, and Fractals, *edited by Francis T. S. Yu and Suganda Jutamulia*
55. Devices for Optoelectronics, *Wallace B. Leigh*
56. Practical Design and Production of Optical Thin Films, *Ronald R. Willey*
57. Acousto-Optics: Second Edition, *Adrian Korpel*
58. Diffraction Gratings and Applications, *Erwin G. Loewen and Evgeny Popov*
59. Organic Photoreceptors for Xerography, *Paul M. Borsenberger and David S. Weiss*
60. Characterization Techniques and Tabulations for Organic Nonlinear Optical Materials, *edited by Mark G. Kuzyk and Carl W. Dirk*
61. Interferogram Analysis for Optical Testing, *Daniel Malacara, Manuel Servin, and Zacarias Malacara*
62. Computational Modeling of Vision: The Role of Combination, *William R. Uttal, Ramakrishna Kakarala, Spiram Dayanand, Thomas Shepherd, Jagadeesh Kalki, Charles F. Lunskis, Jr., and Ning Liu*
63. Microoptics Technology: Fabrication and Applications of Lens Arrays and Devices, *Nicholas Borrelli*
64. Visual Information Representation, Communication, and Image Processing, *edited by Chang Wen Chen and Ya-Qin Zhang*
65. Optical Methods of Measurement, *Rajpal S. Sirohi and F. S. Chau*
66. Integrated Optical Circuits and Components: Design and Applications, *edited by Edmond J. Murphy*
67. Adaptive Optics Engineering Handbook, *edited by Robert K. Tyson*
68. Entropy and Information Optics, *Francis T. S. Yu*
69. Computational Methods for Electromagnetic and Optical Systems, *John M. Jarem and Partha P. Banerjee*
70. Laser Beam Shaping, *Fred M. Dickey and Scott C. Holswade*
71. Rare-Earth-Doped Fiber Lasers and Amplifiers: Second Edition, Revised and Expanded, *edited by Michel J. F. Digonnet*
72. Lens Design: Third Edition, Revised and Expanded, *Milton Laikin*
73. Handbook of Optical Engineering, *edited by Daniel Malacara and Brian J. Thompson*
74. Handbook of Imaging Materials: Second Edition, Revised and Expanded, *edited by Arthur S. Diamond and David S. Weiss*
75. Handbook of Image Quality: Characterization and Prediction, *Brian W. Keelan*
76. Fiber Optic Sensors, *edited by Francis T. S. Yu and Shizhuo Yin*
77. Optical Switching/Networking and Computing for Multimedia Systems, *edited by Mohsen Guizani and Abdella Battou*
78. Image Recognition and Classification: Algorithms, Systems, and Applications, *edited by Bahram Javidi*

79. Practical Design and Production of Optical Thin Films: Second Edition, Revised and Expanded, *Ronald R. Willey*
80. Ultrafast Lasers: Technology and Applications, *edited by Martin E. Fermann, Almantas Galvanauskas, and Gregg Sucha*
81. Light Propagation in Periodic Media: Differential Theory and Design, *Michel Nevière and Evgeny Popov*
82. Handbook of Nonlinear Optics, Second Edition, Revised and Expanded, *Richard L. Sutherland*
83. Polarized Light: Second Edition, Revised and Expanded, *Dennis Goldstein*
84. Optical Remote Sensing: Science and Technology, *Walter Egan*
85. Handbook of Optical Design: Second Edition, *Daniel Malacara and Zacarias Malacara*
86. Nonlinear Optics: Theory, Numerical Modeling, and Applications, *Partha P. Banerjee*
87. Semiconductor and Metal Nanocrystals: Synthesis and Electronic and Optical Properties, edited by *Victor I. Klimov*
88. High-Performance Backbone Network Technology, *edited by Naoaki Yamanaka*
89. Semiconductor Laser Fundamentals, *Toshiaki Suhara*
90. Handbook of Optical and Laser Scanning, *edited by Gerald F. Marshall*
91. Organic Light-Emitting Diodes: Principles, Characteristics, and Processes, *Jan Kalinowski*
92. Micro-Optomechatronics, *Hiroshi Hosaka, Yoshitada Katagiri, Terunao Hirota, and Kiyoshi Itao*
93. Microoptics Technology: Second Edition, *Nicholas F. Borrelli*
94. Organic Electroluminescence, *edited by Zakya Kafafi*
95. Engineering Thin Films and Nanostructures with Ion Beams, *Emile Knystautas*
96. Interferogram Analysis for Optical Testing, Second Edition, *Daniel Malacara, Manuel Sercin, and Zacarias Malacara*
97. Laser Remote Sensing, *edited by Takashi Fujii and Tetsuo Fukuchi*
98. Passive Micro-Optical Alignment Methods, *edited by Robert A. Boudreau and Sharon M. Boudreau*
99. Organic Photovoltaics: Mechanism, Materials, and Devices, *edited by Sam-Shajing Sun and Niyazi Serdar Saracftci*
100. Handbook of Optical Interconnects, *edited by Shigeru Kawai*
101. GMPLS Technologies: Broadband Backbone Networks and Systems, *Naoaki Yamanaka, Kohei Shiomoto, and Eiji Oki*
102. Laser Beam Shaping Applications, *edited by Fred M. Dickey, Scott C. Holswade and David L. Shealy*
103. Electromagnetic Theory and Applications for Photonic Crystals, *Kiyotoshi Yasumoto*
104. Physics of Optoelectronics, *Michael A. Parker*
105. Opto-Mechanical Systems Design: Third Edition, *Paul R. Yoder, Jr.*
106. Color Desktop Printer Technology, *edited by Mitchell Rosen and Noboru Ohta*
107. Laser Safety Management, *Ken Barat*

108. Optics in Magnetic Multilayers and Nanostructures, *Štefan Višňovský*
109. Optical Inspection of Microsystems, *edited by Wolfgang Osten*
110. Applied Microphotonics, *edited by Wes R. Jamroz, Roman Kruzelecky, and Emile I. Haddad*
111. Organic Light-Emitting Materials and Devices, *edited by Zhigang Li and Hong Meng*
112. Silicon Nanoelectronics, *edited by Shunri Oda and David Ferry*
113. Image Sensors and Signal Processor for Digital Still Cameras, *Junichi Nakamura*
114. Encyclopedic Handbook of Integrated Circuits, *edited by Kenichi Iga and Yasuo Kokubun*
115. Quantum Communications and Cryptography, *edited by Alexander V. Sergienko*
116. Optical Code Division Multiple Access: Fundamentals and Applications, *edited by Paul R. Prucnal*
117. Polymer Fiber Optics: Materials, Physics, and Applications, *Mark G. Kuzyk*
118. Smart Biosensor Technology, *edited by George K. Knopf and Amarjeet S. Bassi*
119. Solid-State Lasers and Applications, *edited by Alphan Sennaroglu*
120. Optical Waveguides: From Theory to Applied Technologies, *edited by Maria L. Calvo and Vasudevan Lakshiminarayanan*
121. Gas Lasers, *edited by Masamori Endo and Robert F. Walker*
122. Lens Design, Fourth Edition, *Milton Laikin*
123. Photonics: Principles and Practices, *Abdul Al-Azzawi*
124. Microwave Photonics, *edited by Chi H. Lee*
125. Physical Properties and Data of Optical Materials, *Moriaki Wakaki, Keiei Kudo, and Takehisa Shibuya*
126. Microlithography: Science and Technology, Second Edition, *edited by Kazuaki Suzuki and Bruce W. Smith*
127. Coarse Wavelength Division Multiplexing: Technologies and Applications, *edited by Hans Joerg Thiele and Marcus Nebeling*
128. Organic Field-Effect Transistors, *Zhenan Bao and Jason Locklin*
129. Smart CMOS Image Sensors and Applications, *Jun Ohta*
130. Photonic Signal Processing: Techniques and Applications, *Le Nguyen Binh*
131. Terahertz Spectroscopy: Principles and Applications, *edited by Susan L. Dexheimer*

# Terahertz Spectroscopy

## PRINCIPLES AND APPLICATIONS



Edited by Susan L. Dexheimer

CRC Press
Taylor & Francis Group
Boca Raton London New York

CRC Press is an imprint of the
Taylor & Francis Group, an **informa** business

CRC Press
Taylor & Francis Group
6000 Broken Sound Parkway NW, Suite 300
Boca Raton, FL 33487-2742

© 2008 by Taylor & Francis Group, LLC
CRC Press is an imprint of Taylor & Francis Group, an Informa business

No claim to original U.S. Government works
Printed in the United States of America on acid-free paper
10 9 8 7 6 5 4 3 2 1

International Standard Book Number-13: 978-0-8493-7525-5 (Hardcover)

This book contains information obtained from authentic and highly regarded sources. Reprinted material is quoted with permission, and sources are indicated. A wide variety of references are listed. Reasonable efforts have been made to publish reliable data and information, but the author and the publisher cannot assume responsibility for the validity of all materials or for the consequences of their use.

Except as permitted under U.S. Copyright Law, no part of this book may be reprinted, reproduced, transmitted, or utilized in any form by any electronic, mechanical, or other means, now known or hereafter invented, including photocopying, microfilming, and recording, or in any information storage or retrieval system, without written permission from the publishers.

For permission to photocopy or use material electronically from this work, please access www.copyright.com (http://www.copyright.com/) or contact the Copyright Clearance Center, Inc. (CCC) 222 Rosewood Drive, Danvers, MA 01923, 978-750-8400. CCC is a not-for-profit organization that provides licenses and registration for a variety of users. For organizations that have been granted a photocopy license by the CCC, a separate system of payment has been arranged.

**Trademark Notice:** Product or corporate names may be trademarks or registered trademarks, and are used only for identification and explanation without intent to infringe.

**Library of Congress Cataloging-in-Publication Data**

Dexheimer, Susan L.
Terahertz spectroscopy : principles and applications / Susan L. Dexheimer.
p. cm. -- (Optical science and engineering)
Includes bibliographical references and index.
ISBN 978-0-8493-7525-5 (hardcover : alk. paper) 1. Terahertz spectroscopy. I. Title. II. Series.

QC454.T47D49 2007
543'.5--dc22 2007024954

**Visit the Taylor & Francis Web site at**
**http://www.taylorandfrancis.com**

**and the CRC Press Web site at**
**http://www.crcpress.com**

# Contents

# Preface

The development of new sources and methods in the terahertz, or far-infrared, spectral range has generated intense interest in terahertz spectroscopy and its application in a wide range of fields. Terahertz frequencies, broadly defined as 0.1–30 THz, span the range of low-energy excitations in electronic materials, low-frequency vibrational modes of condensed phase media, and vibrational and rotational transitions in molecules, making this a key spectral range for probing fundamental physical interactions as well as for practical applications. Moreover, the short pulse durations achievable with terahertz techniques based on femtosecond laser sources allow time-resolved measurements on femtosecond timescales, which were previously inaccessible in this spectral range.

This volume provides an up-to-date reference on state-of-the-art terahertz spectroscopic techniques, focusing in particular on time-domain methods based on femtosecond laser sources, and reviewing important recent applications of terahertz spectroscopy in physics, chemistry, and biology. Chapters are contributed by leading experts in each topic. The focus of this book specifically on spectroscopy and the range of applications presented set it apart from the few other recent volumes in the emerging terahertz field. The reader is referred to *Sensing with Terahertz Radiation* edited by Daniel Mittleman (Springer, 2003) and to Terahertz Sensing Technology edited by Dwight L. Woolard et al. (World Scientific, 2003) for applications including ranging and imaging, and *Terahertz Optoelectronics* edited by Kiyomi Sakai (Springer, 2005) for a review focusing specifically on work on generation of terahertz radiation carried out in Japan.

The first section of this book is devoted to instrumentation and methods for time-domain and time-resolved terahertz spectroscopy. The first chapter provides a comprehensive discussion of time-domain terahertz spectroscopic measurements using photoconductive antenna sources and detectors, including methods for determining optical constants from time-domain measurements. The second chapter provides a review of time-domain terahertz techniques based on the nonlinear optical processes of optical rectification for terahertz pulse generation and free-space electrooptic sampling for terahertz pulse detection, and the third chapter reviews current state-of-the-art femtosecond time-resolved techniques and terahertz emission spectroscopy using femtosecond laser sources. Measurements using free electron laser sources and the established far-infrared frequency-domain spectroscopic techniques of FTIR and photomixing are also discussed in the context of specific applications in Sections II and III.

Applications of terahertz spectroscopy to key areas of current interest, both fundamental and applied, are presented in Sections II and III of the book. The second section is devoted to applications in physics and materials science, including studies of carrier processes in state-of-the-art semiconductor materials, superconductors, novel

electronic materials, and semiconductor nanostructures. The third and final section of the book is devoted to applications of terahertz spectroscopy to the biological and chemical fields. This first chapter of this section reviews studies of biologically important molecules, and the final chapter reviews applications of terahertz spectroscopy to pharmaceutical analysis and to the detection of security hazards.

**Susan L. Dexheimer**
**Editor**

# Editor

**Susan L. Dexheimer** received an S.B. degree in Physics from the Massachusetts Institute of Technology and a Ph.D. in Physics from the University of California, Berkeley. She has a broad research background at the interfaces of experimental condensed matter physics, chemical physics, and molecular biophysics. She is currently on the faculty at Washington State University, where her research includes the application of femtosecond optical and terahertz spectroscopic techniques to study ultrafast dynamics in electronic materials and molecular systems.

# Contributors

**Richard D. Averitt**
Department of Physics
Boston University
Boston, Massachusetts

**Jason B. Baxter**
Department of Chemistry
Yale University
New Haven, Connecticut

**Sam G. Carter**
JILA
University of Colorado
Boulder, Colorado

**John Cerne**
Department of Physics
State University of New York at Buffalo
Buffalo, New York

**R. Alan Cheville**
Department of Electrical and Computer Engineering
Oklahoma State University
Stillwater, Oklahoma

**Susan L. Dexheimer**
Department of Physics
Washington State University
Pullman, Washington

**Edwin J. Heilweil**
National Institute of Standards and Technology
Gaithersburg, Maryland

**Robert A. Kaindl**
Lawrence Berkeley National Laboratory
Berkeley, California

**David F. Plusquellic**
National Institute of Standards and Technology
Gaithersburg, Maryland

**Thomas Rades**
School of Pharmacy
University of Otago
Dunedin, New Zealand

**Charles A. Schmuttenmaer**
Department of Chemistry
Yale University
New Haven, Connecticut

**Suranjana Sengupta**
Department of Physics, Applied Physics and Astronomy
Rensselaer Polytechnic Institute
Troy, New York

**Jie Shan**
Department of Physics
Case Western Reserve University
Cleveland, Ohio

**Mark S. Sherwin**
Department of Physics
University of California, Santa Barbara
Santa Barbara, California

**Philip F. Taday**
TeraView Ltd.
Cambridge, United Kingdom

**Ingrid Wilke**
Department of Physics, Applied Physics and Astronomy
Rensselaer Polytechnic Institute
Troy, New York

**J. Axel Zeitler**
Department of Chemical Engineering
University of Cambridge
Cambridge, United Kingdom

# Section I

## Instrumentation and Methods

# 1 Terahertz Time-Domain Spectroscopy with Photoconductive Antennas

*R. Alan Cheville*
Oklahoma State University

## CONTENTS



## 1.1 INTRODUCTION TO TERAHERTZ SPECTRAL REGION

A recent report from the National Academies outlines that electronic and optics are combining to open up a new "Tera-Era."[1] This vision includes computers performing operations at rates of teraflops, terabit-per-second communication systems, and electronic devices on the picosecond time scale. From a spectroscopic point of view, the terahertz (THz) spectral region from 300 GHz ($\lambda = 1$ mm) to 10 THz ($\lambda = 30$ μm) has not yet seen the technological development of optical or microwave frequencies with the result that commercial spectrometers covering the entire spectral range are not yet widely available. This is primarily because of the difficulty of generating and detecting THz frequencies compared with the better-established technologies of optics and electronics.

The so-called "THz gap" arises from the nature of the sources and detectors used in spectroscopy both at the optical (high-frequency) side and electronic (low-frequency) side of the gap. One terahertz corresponds to a photon energy of 4 meV (33.3 $cm^{-1}$). These energies are much less than the electronic state transitions of

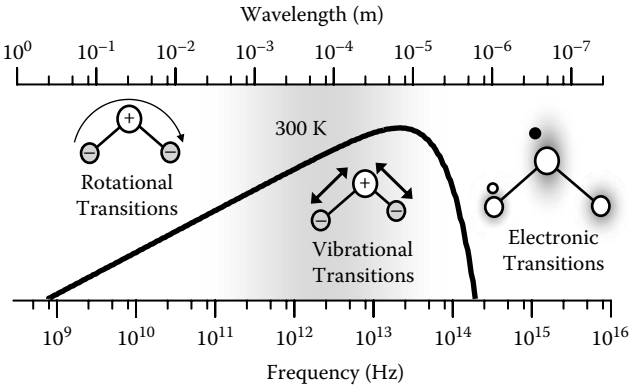


**FIGURE 1.1** The electromagnetic spectrum from microwave to optical region. The area easily accessible by THz spectroscopy using photoconductive sources is shown shaded in gray. Rotational, vibrational, and electronic transitions are shown along with the blackbody radiation curve at 300 K.

atoms and molecules commonly used in lasers or other light sources (Figure 1.1). Semiconductor materials also have bandgaps on the order of an electron volt, orders of magnitude larger than THz energies.

Vibrational frequencies, such as the 10.6 μm $CO_2$ laser, and rotational transition frequencies do fall in the far infrared. Light sources based on these transitions exist, but typically cover limited frequency ranges.[2] Thermal emission from incoherent blackbody radiation is one of the most commonly used sources since the thermal energy, kT, is about 25 meV at room temperature (300 K). The blackbody radiation curve and the relative spectral power emitted are shown as a black line in Figure 1.1. Scaling electronics to operate in the THz gap is limited by the frequency response of devices. The high-frequency limit is determined by the time it takes electrons to traverse the device, which is determined by the physical size and carrier mobility. Although feature sizes are continually shrinking, material properties ultimately limit high-frequency response. New semiconductor materials and the ability to confine carriers at the quantum level are leading to high-speed devices pushing into the THz gap. Some exciting recent developments are laser diodes,[3] high electron mobility transistors, and quantum cascade lasers.[4]

The same physical limitations that arise in scaling optical sources down (or electronic sources up) to the THz spectral region also hold for detectors of THz radiation. THz photons cannot excite electrons into the conduction band in a photodiode (without multiphoton absorption, which would require unreasonable intensities) or provide enough energy to cause photoelectric emission of electrons. Although bolometers can detect radiation, they are limited by incoherent thermal background signals unless cooled to very low temperatures.

The far infrared spectrum and the points made previously are summarized in Figure 1.1. There is a great deal of interest in this spectral region ranging from creating faster electronic devices to the wealth of spectroscopic information available.

THz spectroscopy provides information on the basic structure of molecules and is a useful tool of radio astronomy. Rotational frequencies of light molecules fall in this spectral region, as do vibrational modes of large molecules with many functional groupings, including many biologic molecules that have broad resonances at THz frequencies.

This chapter provides an overview of how the technologic difficulties inherent to THz generation and detection can be overcome through a synthesis of ultrafast optical and electronic techniques. By gating micron scale antennas on photoconductive substrates with femtosecond pulses, it is possible to generate and detect electromagnetic pulses with THz bandwidths.

## 1.2 BRIEF THEORETICAL BACKGROUND FOR PHOTOCONDUCTIVE TERAHERTZ GENERATION

Because THz radiation generated and detected through photoconduction arises from the flow of charge, it is theoretically described by Maxwell's equations. Maxwell's equations do not, however, describe the processes from which charge flow occurs on a femtosecond scale in semiconductors. This is a topic worthy of a complete book,[5] and the description of processes from which charge flow arises are not gone into in detail here. From the perspective of THz generation, the source terms of Maxwell's equations are written to show time-dependent terms explicitly by adding a $(t)$ to them.

$$\nabla \times \vec{E}(t) = \frac{\partial \mu(t)\vec{H}(t)}{\partial t}$$
$$\nabla \times \vec{H}(t) = \sigma(t)\vec{E}(t) + \frac{\partial \varepsilon(t)\vec{E}(t)}{\partial t} \tag{1.1}$$

Here, $\mu(t)H(t) = B(t)$ is the magnetic flux, $H(t) = \sigma(t)E(t)$ is the current density, and $\varepsilon(t)E(t) = D(t)$ is the electric displacement. Any process that creates a time-dependent change in the material properties $\mu$, $\sigma$, or $\varepsilon$ can act as a source term that can result in emission of THz radiation. For THz generation using photoconductive switches, an ultrashort optical pulse incident on a semiconductor causes rapid transient changes to the macroscopic material properties represented by $\sigma(t)$, $\mu(t)$, and $\varepsilon(t)$. For the discussion that follows, the major change caused by the optical pulse is assumed to be in the conductivity, $\sigma$. The rapid, optically induced change of $\sigma$ on a femtosecond time scale is the origin of ultrafast THz pulses generated through photoconduction as well as the physical mechanism by which the THz pulses are detected. It is important to note that many physical processes occur when ultrafast optical pulses are absorbed by semiconductors, and, from an experimental viewpoint, they are not easily separable. Both resonant (absorption of a photon to create charge carriers, $\sigma$) and nonresonant (nonlinear optical difference frequency generation, $\varepsilon$) effects can contribute to THz pulse generation. A common example of a material in which both processes contribute to THz generation is gallium arsenide (GaAs).

The driving term, $\sigma(t)$, in Maxwell's equations results from an ultrafast optical pulse that impulsively excites the semiconductor. The resulting electric and magnetic

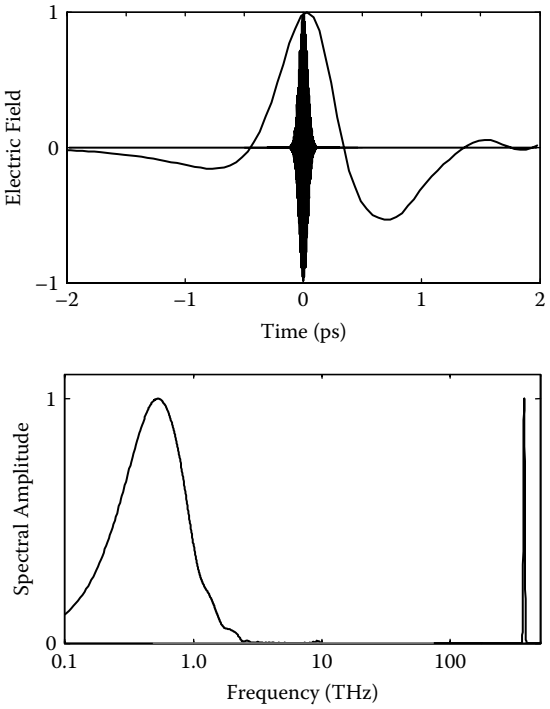


**FIGURE 1.2** Electric field of a measured THz pulse and the simulated field of the exciting optical pulse are shown in the upper figure, whereas the amplitude spectrum is shown in the lower figure.

fields created through the time-dependent conductivity have fast transients with correspondingly broad spectral bandwidths. The spectral bandwidth can be estimated from the uncertain relation [between the bandwidth, $\Delta\omega$, required to support a transient signal] $\Delta t$. Because $\Delta t \Delta\omega \geq ½$, a 1-ps excitation pulse requires, and can create, spectral bandwidths on the order of 0.3 THz, whereas a 100-fs transient has a bandwidth of at least 3 THz. With sub-10-fs pulses readily available from current commercial ultrafast lasers, very broad spectral coverage of the THz region has been achieved.

An example of a THz measurement from the author's laboratory is shown in Figure 1.2. The upper figure compares the measurement of the electric field of a THz pulse in the time domain with the numerically calculated electric field of the 50-fs optical pulse at 800 nm used to generate the THz pulse. The rapidly oscillating carrier frequency of the optical pulse makes it appear to be a filled Gaussian envelope. The spectral amplitude of the THz pulse and optical pulse are shown in the lower figure. Although the actual bandwidth of the optical pulse (10.6 THz) is considerably larger than that of the THz pulse (0.7 THz), the THz pulse spans a greater fraction of the electromagnetic spectrum in terms of $\Delta\nu/\nu_o$: 0.7 for the THz pulse compared to 0.003 for the optical pulse. Recent developments in THz generation and detection

have extended the frequency range spanned by THz pulses by an additional order of magnitude or more. One of the great advantages of ultrafast THz measurements is that this bandwidth allows a broad range of energy scales (frequencies) to be probed in a single measurement with high temporal resolution.

Figure 1.2 highlights some of the differences between short pulses in the THz and optical spectral regions. The electric field of the THz pulse is a nearly single cycle oscillation, whereas the optical pulse is described as a Gaussian pulse envelope superimposed on a sinusoidal carrier frequency. The optical pulse thus meets the slowly varying envelope approximation, whereas the THz pulse does not. Thus many of the simplifying assumptions used in quantum and nonlinear optics do not necessarily apply to THz systems.[6,7] From a theoretical perspective, an accurate description of the pulse propagation requires the solution of the coupled Maxwell-Bloch equations. Because THz pulses used for spectroscopy have very low peak powers compared with optical pulses, nonlinearities can generally be neglected and propagation is treated using linear dispersion theory.[8]

Perhaps the most significant difference between THz pulses and visible, infrared, or ultraviolet light more familiar to most researchers is THz spectroscopy directly measures the electric field of the pulse rather than the intensity. The direct measurement of field is possible simply because of the much slower variation of the field as can be seen in Figure 1.2. Intensity, $I$, and electric field, $E$, are related by:

$$I = \frac{1}{2}\sqrt{\frac{\mu}{\varepsilon}} EE^* \tag{1.2}$$

Equation 1.2 illustrates the well-known fact that intensity measurements contain no phase information unless techniques such as holography or interferometry are used to measure phase relative to another optical beam. The time-resolved electric field of the THz pulse does, however, contain complete phase information that can be extracted directly from THz measurements. For the more familiar intensity measurements, energy conservation dictates that reflection and transmission coefficients are real and positive with magnitude less than one in almost all commonly encountered cases. Because THz experiments measure the electric field amplitude the Fresnel coefficients can be complex and have values less than zero or greater than one. For example, the amplitude transmission coefficient from air to silicon is $t_{12} = 0.45$, whereas that from silicon to air is $t_{21} = 1.55$. Examples will be discussed later.

The final commonly encountered difference between experimental measurements at optical and THz frequencies is the effect of phase shifts on the measured pulse shape. Small changes in the phase of an optical pulse generally have little to no effect on the measured pulse shape. Larger frequency-dependent phase shifts, such as those caused by dispersive media, do result in pulse broadening. In contrast, small-frequency, independent-phase changes result in significant reshaping of THz pulses, as shown in Figure 1.3. Numeric phase changes of 0, $\pi/16$, $\pi/8$, $\pi/4$, $\pi/2$, and $\pi$ result in pulse reshaping up to a complete inversion of the pulse. Such phase shifts can occur on reflection,[9] when the pulse propagates through a caustic,[10] or in propagating through materials with a complex index.

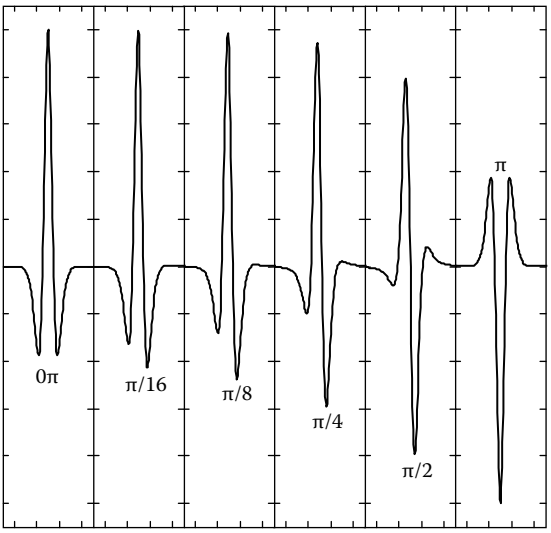


**FIGURE 1.3** Effect of frequency-independent phase shifts from 0 to π/2 radians on the Terahertz pulse shape.

## 1.3 TERAHERTZ-GENERATION PROCESS

Generation and detection of THz pulses occur through nonlinear interaction of the driving optical pulse with a material with fast response. There are two major classifications, of which only one, photoconductivity, is discussed in this chapter. Photoconductive THz generation occurs when optical excitation induces conductivity changes in a semiconductor. This is a resonant interaction and the photons are absorbed through interband transitions. The second mechanism is nonresonant interaction arising from nonlinear frequency mixing or optical rectification. Transient photoconductivity is used for both the generation and detection of THz radiation, with THz generation discussed first.

A simplified representation of the process of photoconductive THz generation is illustrated in Figure 1.4. The six frames of Figure 1.4 represent different steps in pulse generation and are discussed below. A great deal of research continues to be done on understanding the physics underlying THz pulse generation from transient photoconductivity. This area is highly multidisciplinary, integrating knowledge of optical generation of hot carriers, their subsequent rapid thermalization, ballistic transport on a femtosecond time scale, rapid screening of generated fields, design of high bandwidth antenna structures, and propagation of single cycle pulses in dispersive media. Because this chapter focuses primarily on using the pulses in spectroscopic application, only the basic physical fundamentals of THz generation are discussed.[11]

The geometry of a basic photoconductive THz source is shown in a top-down view in Figure 1.4a. A coplanar transmission line is fabricated on a semiconductor substrate with high mobility, μ, usually GaAs or low temperature-grown GaAs.

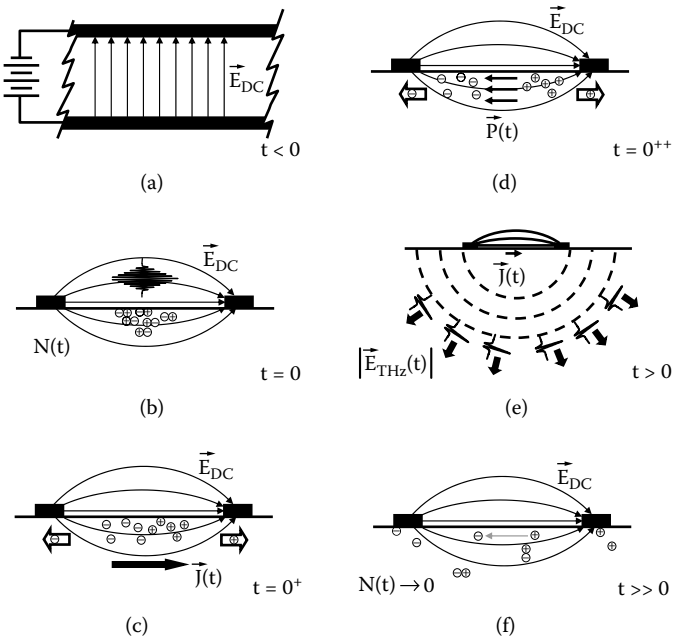


**FIGURE 1.4** Illustration of the process of photoconductive Terahertz generation. Frame (a) shows the coplanar transmission lines before excitation. In (b), the optical pulse generates charge carriers which are accelerated in the static field (c), and create an opposing field in the semiconductor (d). The induced polarization creates a transient current element which radiates a Terahertz pulse (e) followed by recombination back to steady state (f).

Because the mobility gives the ratio of carrier drift velocity to applied electric field, carriers in high-mobility compounds accelerate rapidly, leading to fast rise times. The coplanar transmission lines are DC-biased to produce a field on the order of $10^6$ V/m near the breakdown threshold for air. The electric field near the surface of the semiconductor is represented in the figure by parallel arrows between the lines. Energy is stored by this capacitive structure, with a capacitance on the order of several pF. The semiconductor used has a high dark resistivity to minimize current flow and the resultant local heating and device failure due to electromigration.[12]

The first step in generating THz radiation is optical excitation of the region of high electric field. It is important that the semiconductor bandgap energy, $E_{gap}$, is less than the photon energy, $h\nu$, so that electron-hole pairs are formed. Carrier generation is shown in a cross-sectional view in Figure 1.4b, where dimensions are shown not to scale to better illustrate the physical processes occurring. A focused ultrafast optical pulse incident between the metal lines generates a thin conductive region down to approximately the absorption depth $1/\alpha$. Typical absorption coefficients of semiconductors above the band gap range from $\alpha = 10^3$ cm$^{-1}$ to $\alpha = 10^5$ cm$^{-1}$. The optically generated electron-hole pairs form an electrically neutral plasma near the semiconductor surface as illustrated in Figure 1.4b. The time evolution of the charge

density is given by $N(t)$ with the total carrier density the sum of that of the electrons and holes: $N(t) = N_e(t) + N_h(t)$. At low-excitation fluences, the charge density is proportional to the intensity profile of the optical pulse $I(t)$. The time evolution of the carrier density is given by:[11]

$$N(t) = \int_0^t G(\tau)\delta\tau - N_0 e^{-\frac{t}{\tau_c}} \tag{1.3}$$

where the first term describes $N$(t) at time scales of the laser pulse and the second describes the evolution of the carrier density at longer times. Here $\tau_c$ is the carrier lifetime, $G(\tau)$ is the optical carrier generation rate determined by the optical pulse profile, and $N_o$ is the total number of carriers generated. The free carriers affect the conductivity by $\sigma(t) = N(t)e\mu$. The current density is $J(t) = \sigma(t)E$, which can be written as $J(t) = N(t)ev(t)$ with $v(t)$ the carrier velocity. Immediately after generation of the carriers in the semiconductor the accelerating field is $E(t = 0^+) = E_{DC}$. The time dependence has been written explicitly to illustrate the transient nature of the photoconductivity on subpicosecond time scales. It is the transient current, $J(t)$, that generates the THz pulse.

The carriers are accelerated in the applied electric field, $E_{DC}$, as shown in Figure 1.4c. The time evolution of carrier velocity is determined by the initial acceleration of carriers with effective mass $m^*$ and by rapid carrier scattering with a characteristic time $\tau_s$:

$$\frac{\delta v(t)}{\delta t} = -\frac{v(t)}{\tau_s} + \frac{e}{m^*}E(t)$$

The carrier scattering time is determined by phonon scattering, carrier scattering, scattering from dopants, and the photon energy, or where in the conduction band carriers are generated.

The spatial separation of the photo-induced electron and hole plasma create a macroscopic polarization, $P(t)$, in the semiconductor, shown in Figure 1.4d. The polarization is given by $P(t) = N(t)er(t)$, where $r(t)$ is the spatial separation of charges. The time evolution of the induced polarization is calculated from:

$$\frac{\delta P(t)}{\delta t} = -\frac{P(t)}{\tau_R} + N(t)ev(t) \tag{1.4}$$

where the time derivative of the polarization is $N(t)ev(t)$. As shown in Figure 1.4d, the induced polarization creates an electric field that opposes the static field of the biased coplanar stripline. The electric field responsible for carrier acceleration then evolves as:

$$E(t) = E_{DC} + \frac{P(t)}{\varepsilon\gamma} \tag{1.5}$$

where $\gamma$ is a numerical factor that depends on the geometry. The four coupled differential equations describing the carrier density $N(t)$, the velocity $v(t)$, the polarization $P(t)$, and the electric field seen by the carriers $E(t)$ describe the time evolution of the current created by photo-excitation of a carrier.[11]

The THz pulse is generated from the transient current element, $J(t)$, shown in Figure 1.4e on a greatly expanded spatial scale. Generation of a pulse follows directly from Maxwell's equations because time varying current serves as a source term:

$$\nabla \times \vec{E}_{THz}(t) = -\mu \frac{\partial \vec{H}_{THz}(t)}{\partial t}$$
$$\nabla \times \vec{H}_{THz}(t) = \vec{J}(t) + \frac{\partial \varepsilon(t) \vec{E}_{THz}(t)}{\partial t} \tag{1.6}$$

where the subscript THz distinguishes the time resolved THz field from the field in the semiconductor. Maxwell's equations with these terms and those described in the next paragraphs are generally not amenable to analytic solution. Because many experimental techniques of THz generation focus the optical spot to micron diameters to generate large carrier densities, the current element is typically much smaller than one wavelength of the generated THz radiation and thus can be described as a Hertzian dipole.[13] The calculations are complicated by the fact that the current element is on the surface of a dielectric half space, but both analytic and numerical solutions exist for dipole antennas on dielectric half spaces.[14] The major fraction of the laser-generated burst of THz radiation is emitted into the semiconductor by a factor proportional to $n^3$ where $n$ is the index of refraction of the semiconductor. Because most semiconductors have refractive indices higher than three at THz frequencies, this is a significant enhancement in directivity and aids in collection and collimation of the THz radiation. When the optical excitation spot is not tightly focused so the current distribution is on the same order of a wavelength or larger, the problem is often treated as a summation (array) of small radiating elements. Because the current rises and falls on a time scale of one picosecond, it generates a well-defined pulse front that propagates outward from the optical excitation point. The radiation pattern is changed by the proximity of the dipole to the air–semiconductor interface and will be discussed later.

All these processes happen on time scales of picoseconds or less. On longer time scales, carrier recombination within the semiconductor or at the metal electrodes causes the induced polarization to decay and the static bias electric field to reestablish itself, This is illustrated in Figure 1.4f. The recovery of the semiconductor to the state shown in Figure 1.4a typically takes hundreds of picoseconds or longer.[11]

In summary, a DC-biased semiconductor (a) has an electron-hole plasma created on femtosecond time scales by an optical pulse (b). The rapid acceleration and separation of the electrons and holes create a current transient (c). The macroscopic polarization creates an opposing field that screens the DC field (d). The transient electric field determined (approximately) by the time derivative of the current results in a radiated pulse front (e). In times of hundreds of picoseconds, the semiconductor recovers (f).

Considerable research has gone into development of photoconductive THz emitters for specific applications. The simple coplanar stripline structure of Figure 1.4 can be replaced by an array of antenna structures. Log-spiral, bowtie, and a variety of dipole structures have all been developed. In this case, the photocurrent provides an impulse excitation to the antenna and the radiation pattern and THz pulse are determined both by the response of the semiconductor as well as the antenna. Biased antenna structures are not required to generate photoconductive THz radiation. The electric field that arises from depletion of carriers from recombination centers near the surface will accelerate photo-induced carriers away from or toward the surface. In this case, the induced electric dipole is normal to the surface, rather than in the plane of the surface as with antenna structures, which makes it more difficult to couple radiation out of the substrate. The photo-Dember effect[15] can also give rise to THz radiation. The Dember effect arises from the difference in mobility between electrons and holes, which causes the carriers accelerate at different rates.

## 1.4 DETECTING TERAHERTZ RADIATION USING PHOTOCONDUCTIVE ANTENNAS

Detecting THz pulses using photoconductively gated antennas relies on the same physical principles as generation of THz pulses, namely ultrafast pulse excitation in a semiconductor causing rapid changes in conductivity. To detect THz pulses with subpicosecond resolution, a micron-scale dipole antenna is fabricated on a semiconductor substrate with a very short carrier lifetime of 1 ps or less. Both the antenna design and properties of the semiconductor critically affect THz detection. A typical antenna structure is shown in Figure 1.5d from a top-down view. The antenna is a center-excited dipole fabricated between coplanar strip lines with length, $h$, of 10 to 200 μm. The length is the most critical element of the antenna and will be discussed later. The antenna's width is tens of microns with a center gap of less than ten microns corresponding to approximately the diameter of the focused gating laser pulse. Typical dark resistance (no optical excitation) of these antenna structures is on the order of megaohms and depends on the substrate resistivity and antenna and coplanar stripline dimensions.

The photoconductive detection process is illustrated schematically in Figure 1.5a–c. Figure 1.5a is a side-on view that illustrates the ultrafast laser pulse (not to scale, see Figure 1.2) incident from the left on the antenna of Figure 1.5d. A THz pulse is propagating from the right, but has not yet arrived at the antenna structure. As in generation of THz pulses, the ultrafast laser pulse generates an electron and hole plasma which decreases conductivity of the antenna gap. The time resolved change in conductivity is $\sigma(t) = N(t)e\mu$, where $N(t)$ is given by Equation 1.3 and $\mu$ is the semiconductor mobility. The arrival of the laser pulse is analogous to closing a switch, which allows the antenna gap to conduct. The short recombination time $\tau_c$ of the semiconductor causes the gap resistance to change from nearly insulating to conducting (closing the switch) then back to insulating (opening the switch) on a picosecond time scale.

The coplanar strip line is connected to a high-sensitivity current amplifier that detects any current flow through the antenna gap with subpicoamp resolution. If the

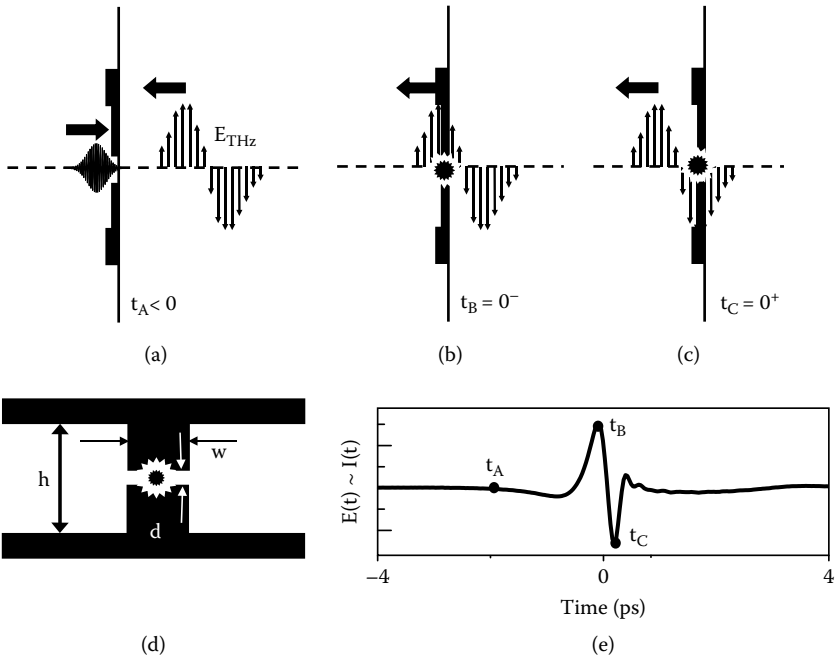


**FIGURE 1.5** Illustration of the process of THz detection. The THz antenna of frame (d) is shown in cross section in frames (a–c). The electric field measurement is determined by the relative arrival times of the optical and THz pulse. In (a), the optical pulse arrives before the THz pulse. By delaying arrival of the optical pulse to coincide with the THz pulse as shown in (b) and (c), the measured current (e) maps out the THz field in time.

resistance of the metal lines is negligible the resistance of the antenna is determined by the antenna gap. The gap resistance is $R(t) = w/\sigma(t)A$, where the cross-sectional area, $A$, is approximately $2d\alpha$ with $\alpha$ the absorption depth in the semiconductor; typically $d >> \alpha$. The current flow from Ohm's law is $I(t) = V(t)/R(t)$, where the antenna bias voltage is provided by the THz pulse: $V(t) \cong E_{THz}(t)h$. In Figure 1.5a, the THz pulse has not yet arrived at the antenna, the bias voltage is zero, and there is no net current flow through the antenna. This is illustrated in Figure 1.5e at the point labeled $t_A$, which occurs at $t < 0$.

Figure 1.5b shows a point later in time; the time axis is determined by the delay between the laser pulse that generates the THz pulse and the pulse that gates the THz antenna. The positive gating peak of THz pulse is incident on the antenna at the same time the optical gating pulse arrives. In this case, $E_{THz} > 0$, and current flows from the lower half of the antenna to the upper are determined by the electric field direction. The measured time average current at point $t_B$ in Figure 1.5e is proportional to the THz electric field. After the current is measured, the delay between the laser generating and gating pulses is again changed to advance the THz pulse in time. Figure 1.5c and point $t_C$ in Figure 1.5e both correspond to a point on the pulse where the electric field is opposite in sign to Figure 1.5b. The time resolved

measurement of the THz pulse electric field is thus made by changing the delay between the optical gating pulse and generating pulse.

From this discussion, it is clear that, to measure the electric field with high temporal resolution, the response time of the semiconductor $\tau_C$ must be short compared with the rate of change of the THz field. Because to a first approximation $\sigma \sim \mu$, semiconductors with both high mobility and short carrier lifetimes are optimal. The two semiconductor materials most commonly used for photoconductive THz detectors are low temperature-grown GaAs and ion implanted silicon on sapphire. Low temperature-grown GaAs has a thin layer grown on a GaAs substrate with the substrate temperature determining the recombination time.[16] Recombination times of hundreds of femtoseconds or less have been reported. Silicon on sapphire is a thin (~1 μm) layer of silicon grown on a sapphire wafer with a reduction of carrier lifetime achieved through ion implantation. The carrier lifetime is dependent on implantation dosage to a point at which it saturates at about 500 fs.[17]

The response time can be estimated by the convolution of the THz pulse electric field, $E_{THz}$, with the detector response time determined by $\sigma(t)$. With the optical gating pulse arriving at t = 0 and the THz pulse at $t = t_o$, the time average current is:

$$I(t) = \frac{2hr\alpha}{w} \int_{-\infty}^{\infty} \sigma(t) E_{THz}(t - t_0 - \tau) \delta\tau \tag{1.7}$$

where the antenna dimensions have been used to estimate the resistance. Equation 1.7 indicates that photoconductors with infinitely short response times excited by infinitely short optical pulses (i.e., a delta function response) are required to exactly measure the time-resolved THz electric field. Although in general short carrier lifetimes allow the faster THz field transients to be measured, there is a tradeoff in actual performance because short lifetimes arise from a high density of trap or defect states that reduce the semiconductor mobility. Additionally, the average current is proportional to the time integral of $\sigma(t)$ so that fast recombination times can lead to lower average current measurements for a given THz field strength. In practice, measuring THz pulses with high-frequency components is more dependent on the laser excitation pulse than the carrier lifetime. This can be understood qualitatively through Equation 1.7 because both step functions and delta functions result in a non-zero average current. The extraction of accurate material parameters for non-ideal measurements of $E_{THz}(t)$ is discussed later.

This section concludes with a brief discussion of the THz antenna structure. Although Equation 1.7 indicates that an increase in the dipole size, $h$, allows high average currents, this is true only if the antenna length remains much less than the THz wavelength (Hertzian dipole). Longer antenna lengths have resonances and exhibit strong frequency dependence. Because the incoming THz pulse in most cases is incident through the semiconductor substrate, the wavelength of the THz radiation is reduced compared with free space by $\lambda_o/n$. Silicon, GaAs, and sapphire have high refractive indices in the THz region, so at frequencies near 1 THz, the wavelength at the antenna is on the order of 100 μm. A large number of antenna designs have been used both for generation and detection of THz radiation beyond simple dipoles. These include log-spiral[18] and bow-tie[19] designs.

### 1.4.1 THz Spectroscopy Using Photoconductive Antennas

This section provides an overview of spectroscopic measurements using photoconductive sources and detectors of THz pulses. Much of the discussion also applies to other ultrafast THz generation and detection techniques such as those based on nonlinear optics covered elsewhere in this book. Photoconductive THz pulses offer unique capabilities for spectroscopic measurements in the far infrared spectral region compared with other techniques such as Fourier transform infrared spectroscopy or techniques such as frequency mixing originally developed at microwave frequencies. This section is intended to provide a brief overview of both the advantages and disadvantages of ultrafast THz spectroscopy, describe the basic theory of extracting spectroscopic information from experimental measurements, and discuss experimental considerations of the technique that can affect the spectroscopic measurements. This section also is intended to provide an overview for the researcher looking to use THz pulses for their own spectroscopic measurements and is thus general rather than specific in the material covered.

The first question to ask is whether THz spectroscopy is the appropriate technique for a given measurement. The THz spectral region accessible via ultrafast optical pulse generation and detection extends from less than 0.1 THz to more than 30 THz. Some source and detector techniques have enhanced low-frequency response, whereas other techniques are used to achieve high frequencies. Both the high- and low-frequency limits have associated experimental difficulties. The low-frequency end of this spectral region extends to frequencies that are easily achievable using high-precision electronic instruments. In addition, long temporal scans are required. For the high-frequency limit above about 10 THz, highly mature optical spectroscopy techniques such as Fourier transform spectroscopy exist. In brief, the choice to use time-resolved THz spectroscopy techniques depends on specific applications. The advantages of time-resolved THz spectroscopy are: coverage of more than a decade frequency range with a single measurement, peak spectral response in the 0.3–3.0 THz spectral range, and the ability to measure phenomena with subpicosecond time resolution.

The THz spectral region is rich in spectroscopic features. Chapters later in this book provide much more complete reviews of the types of systems that can be probed with such pulses. From the perspective of trying to set up a system to perform measurements, THz spectroscopy can be broadly separated into measurement of gases and that of liquids and solids. At the low number density characteristic of gases, the frequency of collisions between molecules determines dephasing times that occur on time scales generally much longer than 1 ps. Spectral features are then less than 1 THz in width and can be less than 1 MHz at low pressures with $Q$ ($\Delta\nu/\nu_o$) of $10^6$ or more. In this limit, time-resolved THz spectroscopy resolves individual transitions over a broad range of energies, but does not have the frequency resolution to measure extremely narrow line widths. Limitations on frequency resolution are discussed in detail later. For liquids and solids resonances are broadened on femtosecond timescales resulting in broad, featureless spectra with corresponding to $Q < 1$ in most cases. For such systems, the spectral width of the short pulse-based measurement techniques can prove extremely valuable. Free carrier absorption occurs

in semiconductor materials in the THz spectral range and the broad spectral coverage is extremely useful for determining material properties. One other difference between THz spectroscopy and spectroscopic techniques at optical frequencies is that the energies of THz photons correspond to thermally accessible energy states. At room temperature the thermal energy, $kT$, corresponds to 25 meV, 208 $cm^{-1}$, or a frequency of 6.25 THz. Thus THz spectroscopy using photoconductive antennas typically covers the region $kT > h\nu$ where thermal energies are higher than photon energies and can probe states that are populated at room temperature. Using short excitation pulses to achieve high frequencies, it is also possible to simultaneously measure the region $h\nu > kT$.

The technique of THz time domain spectroscopy measures the change between time-resolved electric fields of THz pulses propagating through a sample and an equivalent length of free space. Depending on the sample geometry, the change in the THz pulse shape permits either analytic or numeric calculation of the complex sample index, permittivity, or conductivity. One assumption in the following treatment of THz time domain spectroscopy is that the interaction of an electric field with a sample is linear. Maxwell's equation, and Equation 1.1, which describes propagation through a material with constituent parameters given by the permittivity and permeability, is linear for small electric field when higher order terms of the susceptibility can be ignored. THz pulses generated in the laboratory typically have peak powers on the order of 1 $\mu Wcm^{-2}$ corresponding to an electric field on the order of 1 $Vcm^{-1}$.

Because the assumption of linear interactions in most materials is a good one, linear dispersion theory[8] is used to represent the time domain pulse in the frequency domain as a superposition of plane waves of frequency ω, all with a k vector along the THz system optical axis, $z$. The relative amplitude and phase of each plane wave component of the THz pulse are obtained through a Fourier transform of the time-resolved electric field:

$$E(z,\omega) = \frac{1}{2\pi}\int_{-\infty}^{\infty} E(z,t)e^{-i\omega t}\partial\tau \tag{1.8}$$

Here $E(z,\omega)$ is the complex field amplitude and $E(z,t)$ is the experimentally measured THz pulse electric field in the time domain.

A typical measurement of two THz pulses is shown in Figure 1.6. The three frames on the left correspond to the reference pulse that has propagated through free space—in this case, nearly dry air. The three frames on the right correspond to the pulse that has propagated through the sample—humid air containing approximately 1 percent water vapor. The experimentally measured pulses are in the top two frames. The effect of water vapor on the THz pulse in the measurements of Figure 1.6a are visible as oscillations after the pulse. Figure 1.6b shows the magnitude of the complex spectral amplitude obtained through a numeric Fourier transform. Comparing the two spectral amplitudes, the discrete rotational transitions of $H_2O$ can be seen as distinct absorption lines. The relative phase of the plane wave components that make up the two THz pulses is displayed as modulo $2\pi$ in Figure 1.6c. As can be seen from

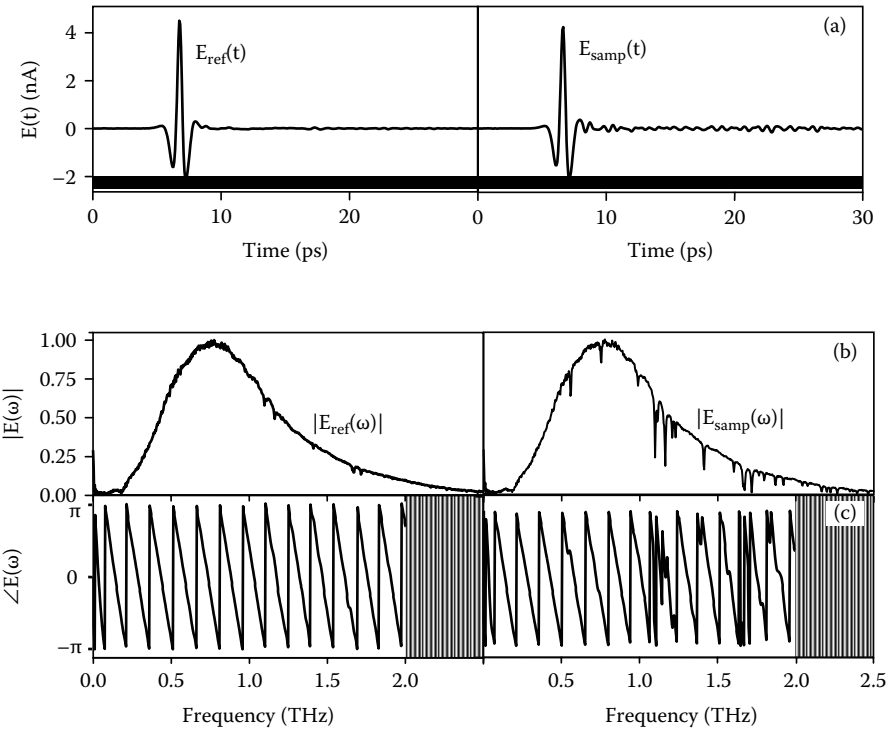


**FIGURE 1.6** The reference and sample pulses discussed in the text are shown in (a) for dry and humid air. Numerical Fourier transforms of the amplitude and phase, (b) and (c), respectively, illustrate the effect of the sample on the plane wave components that comprise the THz pulse.

the figure, the phase changes linearly except near the resonance of the water vapor rotational frequencies. The gray regions on the plot correspond to invalid phase data caused by the reduced spectral amplitudes beyond 2 THz.

Obtaining the complex electric field amplitude spectrum via a Fourier transform permits determination of the complex amplitude after propagating a distance $\Delta z$ through a sample. Given the measured spectrum at the input of the sample, $z = 0$, the field exiting the sample is given by:

$$E(\Delta z, \omega) = E(0, \omega) e^{-ik(\omega)\Delta z} \tag{1.9}$$

The complex k vector, $k(\omega)$, expresses complete information about the THz pulse interaction with the sample material. The wave vector $k(\omega)$ can be expressed several ways, most commonly through the complex index, $n(\omega) = n'(\omega)\text{-}jn''(\omega)$ with $k(\omega) = \omega n(\omega)/c$. The complex index is related to the permittivity through $\varepsilon_r(\omega) = n(\omega)^2$. The imaginary term is related to the power absorption coefficient by $\alpha_p(\omega) = 2\omega n''(\omega)/c$.

The choice of sign for the imaginary term of $n(\omega)$ is made so that plane waves are attenuated and not amplified. The complex, frequency-dependent k vector is then:

$$k(\omega) = \frac{\omega}{c} + \frac{\omega[n'(\omega) - 1]}{c} - \frac{i\alpha_p(\omega)}{2} \tag{1.10}$$

where the first term, $k_0 = \omega/c$, corresponds to the phase change of the THz pulse through a length of free space equivalent to the sample thickness. The reason for expressing the wave vector in this form will be made clear later.

To measure the complex refractive index of the sample, a measurement is first done without the sample in place and with the spectrometer purged with dry air to ensure $n = 1$ along the THz pulse path. The measured THz pulse, $E_{ref}(t)$ in Figure 1.6a, is numerically Fourier transformed to obtain $E_{ref}(\omega)$. The measured THz pulse in a general sense can be written as:

$$E_{ref}(\omega) = E_{gen}(\omega)T(\omega)H(\omega) = E_{gen}(\omega)T(\omega)e^{-ik_0\Delta z} \tag{1.11}$$

where $E_{gen}(\omega)$ is the THz pulse generated by the source, $T(\omega)$ is the frequency response of the THz spectrometer including the THz source and detector, and $H(\omega)$ is the response function of the sample. For the reference sample of length $\Delta z$ of free space, $H(\omega) = exp(-ik_o\Delta z)$. The concept of a transfer function is drawn from engineering and describes the effect of a system on a complex input signal. The terms $E_{gen}(\omega)$ and $T(\omega)$ are not directly measured and depend on numerous experimental parameters and the THz source and detector used.

After the sample is placed into the system, the measured pulse that has propagated through the sample is

$$E_{samp}(\omega) = E_{gen}(\omega)T(\omega)H(\omega) = E_{gen}(\omega)T(\omega)e^{-ik(\omega)\Delta z} \tag{1.12}$$

The material response is determined by dividing the complex amplitude spectrum of the sample pulse by the free space pulse

$$\frac{E_{samp}(\omega)}{E_{ref}(\omega)} = \frac{E_{gen}(\omega)T(\omega)e^{-ik(\omega)\Delta z}}{E_{gen}(\omega)T(\omega)e^{-ik_0\Delta z}} = e^{-i(k(\omega)-k_0)\Delta z} \tag{1.13}$$

As can be seen from the $k(\omega)$-$k_o$ term of Equation 13, division of the sample spectrum by the reference spectrum effectively removes the effect of an equivalent length of free space. The absorption coefficient and index of refraction can be determined from the magnitude and phase of the spectral ratio using Equation 1.10. The refractive index and absorption coefficient of the time domain measurements of humid air, Figure 1.6, are shown in Figure 1.7. The complex index of the rotational transitions have the form of the quasi-Lorentzian line shape with phase and magnitude similar to that of a harmonic oscillator.[20] Besides permitting direct measurement of the

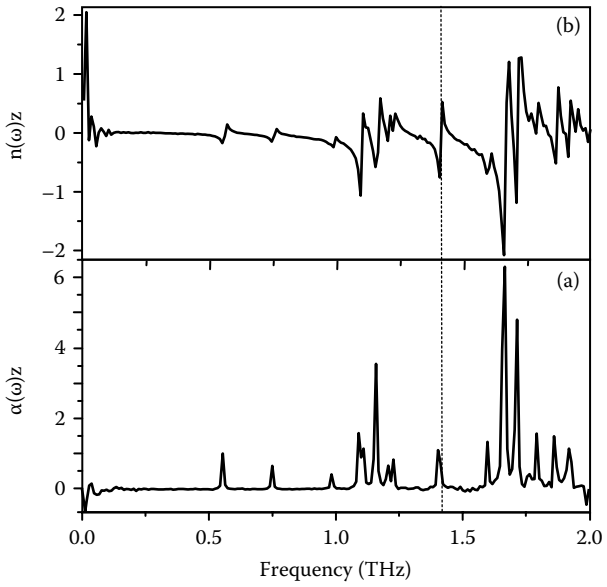


**FIGURE 1.7** Refractive index and absorption coefficient extracted from the data of Figure 1.6.

index and absorption, dividing the Fourier transforms of the measured pulses in the frequency domain is mathematically equivalent to a time domain deconvolution to remove the frequency response of the generated THz pulse and optical system from the sample response function. The effect of this deconvolution is one reason that the response time of the semiconductor does not need to be much shorter than the rate of change of the THz field to perform high-resolution THz spectroscopy.

The formalism of the transfer function in the derivation above is useful because most samples measured with THz time domain spectroscopy do not have simple transfer functions. The derivation previously considered propagation in which the Fresnel reflection and transmission coefficients can be ignored. A more general case is the measurement of a finite thickness of material with index $n_2(\omega)$ surrounded by a material of index $n_1(\omega)$, usually air, so $n_1 = 1$. In this case the Fresnel coefficients need to be taken into account and the transfer function $H(\omega)$ is then defined as:[21]

$$H(\omega) = \frac{t_{12}t_{21}e^{i\beta}}{\left(1 - r_{12}r_{21}e^{i2\beta}\right)} \tag{1.14}$$

where $t_{12}(\omega)$, $t_{21}(\omega)$, $r_{11}(\omega)$, and $r_{21}(\omega)$ are the Fresnel transmission and reflection coefficients[21] and depend on the index of the sample, $n_2(\omega)$. $\beta = n_2 k_o d\cos\theta$ is the phase delay associated with multiple reflections inside the slab where $\theta$ is the angle of propagation inside the slab determined from Snell's law. Although there are no